Fault Ride-Through Enhancement of DFIG-Based Wind Generation Considering Unbalanced and Distorted Conditions

Andres E. Leon, *Graduate Student Member, IEEE*, Juan Manuel Mauricio, *Member, IEEE*, and Jorge A. Solsona, *Senior Member, IEEE*

***Abstract*—A control strategy is proposed to enhance the operation, under network disturbances, of a wind turbine driven doubly fed induction generator (DFIG). The scheme allows us to overcome low voltages, imbalances, and harmonic distortions at the point of common coupling. The control law is designed using a feedback linearization approach plus resonant filters; this law directly controls the DFIG stator powers from the rotor voltages, unlike the most used nested two-loop approaches. An accurate control of the active and reactive powers delivered to the grid permits us to fulfill severe grid code requirements and to improve the fault ride-through capability. Under unbalanced conditions, the reference currents of both grid- and rotor-side converters are coordinately chosen to simultaneously eliminate the double-frequency pulsations in the total active power and electromagnetic torque. Several tests and disturbances to provide a realistic assessment and validation have been performed, showing the adequacy of the proposed controller. Comparisons with other control approaches with different objectives are also presented to illustrate the advantages regarding elimination of the double-frequency ripples and harmonic rejection capability.**

***Index Terms*—Distorted voltage, fault ride-through (FRT) capability, feedback linearization, grid code, resonant controller, wind energy conversion system (WECS).**

I. Introduction

VARIABLE-SPEED wind turbines based on doubly-fed induction generators (DFIGs) are nowadays an extended and mature technology [1], while wind energy conversion systems (WECSs) are increasing their participation in the power generation matrix displacing conventional fossil-fuel generators. In order to prevent possible adverse effects (transient stability, power quality, and system inertia reduction) produced by the high wind power penetration, network operators are ever-increasing the grid code requirements, assigning several network support tasks to WECS [2], [3], such as more severe fault ride-through (FRT) capabilities, additional reactive power injection to the grid [4], short-term frequency regulation (transiently releasing active power [5], [6]), stability enhancement [7], and oscillation damping [8]. For all these functionalities, a more precise control of the DFIG stator active and reactive powers is required.

On the other hand, WECS are usually located in rural areas, far away from strong grid buses where wind resources are abundant, so that the WECS point of common coupling (PCC) often presents unbalanced and distorted voltages [9]. Unbalanced voltages cause several drawbacks in the DFIG wind turbine [10]. First, due to the low negative-sequence impedance of a DFIG, high negative-sequence currents flow in the stator resulting in overcurrents and overheating. Second, the interaction of negative-sequence voltages with positive-sequence currents produces a sustained double-frequency (2ω) pulsation in the electric power and electromagnetic torque. These pulsations are not negligible and generate a high stress in the turbine mechanical system, contributing to the gearbox fatigue or even to the damage of the rotor shaft, gearbox, or blade assembly [11]. These electrical and mechanical problems, beyond a certain amount of imbalance, can activate DFIG protections and disconnect the windmill [12], [13]. Apart from imbalances, harmonics can also be present in a weak electrical network. If the controller does not take into account these voltage harmonics, then stator currents will be distorted as well, along with an increase in the machine copper and iron losses. Considering that power quality standards demand that harmonic-free currents must be delivered to the grid, then both imbalance and harmonics have to be properly addressed in the controller design stage.

II. Background

A. Classical Control Strategies for DFIGs

Direct torque control (DTC), direct power control (DPC), and vector control (VC) [14] are among the most widespread strategies for DFIGs. Some disadvantages of the DTC strategy are that its success depends on an accurate estimation of the instantaneous electrical torque and rotor flux, and that it is influenced by machine parameter variations. Since the DPC relies on a few signal measures, sensors need to be precise and so DPC has low robustness to measurement noise. Both DTC and DPC strategies must have a small control sampling time and large sensor bandwidth to be inside their defined hysteresis bands. On the other hand, although the VC is more complex to implement than DTC and DPC algorithms, the inclusion of proportional-integral (PI)

Manuscript received December 19, 2011; revised April 20, 2012; accepted June 11, 2012. Date of publication June 26, 2012; date of current version July 27, 2012. This work was supported in part by Universidad Nacional del Sur, Consejo Nacional de Investigaciones Científicas y Técnicas (CONICET) and Agencia Nacional de Promoción Científica y Tecnológica (ANPCyT), Argentina, and in part by the Spanish Ministry of Education and Science (MEC) and Junta de Andalucía under Grant ENE2011-24137 and Grant P09-TEP-5170, respectively. Paper no. TEC-00657-2011.

A. E. Leon and J. A. Solsona are with Instituto de Investigaciones en Ingeniería Eléctrica (IIIE) "Alfredo Desages" (UNS-CONICET), Universidad Nacional del Sur (DIEC-UNS), 8000 Bahía Blanca, Argentina (e-mail: aleon@ymail.com; jsolsona@uns.edu.ar).

J. M. Mauricio is with the Department of Electrical Engineering, University of Seville, 41092 Seville, Spain (e-mail: j.m.mauricio@ieee.org).

Digital Object Identifier 10.1109/TEC.2012.2204756

controllers increases its robustness to unmodeled dynamics, parameter variations, and measurement noise [14]. For this reason, VC has some advantages over DTC and DPC, being more used in DFIG applications and studies [15].

B. Straight-Line and Nested Control of DFIG Stator Powers

Several approaches control the stator powers in a cascade way by controlling the rotor currents (see [10], [11], [16]–[22]). First, a fast inner rotor-current control is designed, and then an outer stator-power control is implemented. Any major interaction between both nested control loops is prevented by designing the outer stator-power loop to respond more slowly than the inner rotor-current loop. On the other hand, a faster stator-power control can be made by choosing a straight-line control from the rotor voltages to the stator powers [23], which avoids interaction between nested inner and outer loops, and allows easy control tuning.

Even though the straight-line control approach involves more mathematical operations, it presents several advantages regarding the control performance of the stator powers. However, an obstacle arises when it is attempted to control directly the stator active and reactive powers. As is mentioned in [23] and [24], the marginal stability of the DFIG zero dynamics avoids the implementation of an input–output control when an exact direct inversion is made (for instance, from rotor voltages to stator powers). This internal dynamics has an oscillatory behavior and it is not appropriate for practical implementations. For this reason, most of the DFIG approaches are based on the aforementioned nested two-loop structure. Nevertheless, this obstacle can be overcome by using a simplified second-order model, instead of the full fourth-order model when the DFIG electrical dynamics is considered in the controller design. A control law based on feedback linearization is proposed in [25] with the rotor slip and the terminal voltage as control outputs. However, as explained previously, to properly fulfill grid codes and additional network support tasks we choose the DFIG active and reactive powers as control outputs.

C. Unbalanced and Distorted Voltage Conditions

In the past years, several works have introduced strategies to deal with unbalanced conditions in DFIG-based WECS [10]–[13], [18], [19], [26], [27]. They can be classified into the following categories: the first approach [10], [13], based on a dual VC, independently controls the positive- and negative-sequence currents in two different reference frames; the second category [11], [19], [26] uses a proportional plus resonant controller which allows tracking constant and sinusoidal references without steady-state error. A main-auxiliary control strategy is also presented in [18], whereas other alternative schemes are proposed in [12] and [27]. However, all of these control strategies are based on the nested two-loop control approach. On the other hand, papers on strategies which directly control the DFIG stator powers [23] do not introduce controllers to overcome unbalanced conditions.

In addition, when a controller able to ride through unbalanced conditions is designed, several objectives have to be taken into account. The main target of a controller under imbalances is to nullify the 2ω pulsations in both the total active power delivered to the grid and the DFIG electromagnetic torque. This is simultaneously accomplished only if a coordinated control between the grid- and rotor-side converters is considered [13], [18], [26]. When converter coordination is not developed, only one of the 2ω pulsations can be mitigated, as it was done in [10]–[12], [19], [27]. An additional advantage arises when 2ω pulsations in the total active power and electromagnetic torque are simultaneously nullified, named that the 2ω pulsations in the dc-link voltage are also largely reduced.

The aforementioned works only consider unbalanced voltages, and do not take into account the presence of voltage harmonics in their control proposals. These harmonics make distorted currents to be delivered to the grid, drawback that can be overcome by adding resonant filters for each harmonic in the controller design. This was implemented in [28], where a nested two-loop control was used and imbalances were not considered.

D. Summary of the Features of the Proposed Control

1) Straight-line control from the rotor voltages to the DFIG stator powers is attained, unlike the most used nested two-loop control.
2) Under unbalanced conditions, the 2ω pulsations in the total WECS active power and the DFIG electromagnetic torque are simultaneously nullified, reducing the dc-link voltage oscillations as well.
3) A large FRT capability is achieved, along with an accurate reactive power injection under low voltage events.
4) Harmonic-free currents are delivered to the grid when voltage harmonics arise at the PCC bus.
5) A more robust synchronization is accomplished by using a voltage-oriented approach, unlike the field-oriented approach which needs a precise flux estimation.
6) The controller tuning is carried out in the discrete-time domain, which makes its implementation in digital signal processors easier.

III. DFIG Modeling

The DFIG-based WECS is schematically represented in Fig. 1. The considered wind turbine mechanical system consists of two lumped masses (the wind turbine and the electric rotor) connected through a nonrigid shaft [16]. As mentioned, the DFIG electrical system can be represented by a second-order dynamic model obtained from the full fourth-order model, which is accomplished by neglecting the stator-flux dynamics $\dot{\boldsymbol{\psi}}_{dq} \cong 0$, as justified in [29] and [30]. This second-order electrical model in a synchronous reference frame, in a per unit system, can be written as follows (see [25], [29]–[31]):

$$\tau_0' \dot{e}_q' = -e_q' + (L_s - L_s')\, i_d - \tau_0' e_d' \Omega_B \Delta\omega - e_{rd} \quad (1)$$

$$\tau_0' \dot{e}_d' = -e_d' - (L_s - L_s')\, i_q + \tau_0' e_q' \Omega_B \Delta\omega + e_{rq} \quad (2)$$

where $\mathbf{i}_{dq} = i_q + j i_d$, $\mathbf{e}_{rdq} = e_{rq} + j e_{rd}$, and $\mathbf{e}'_{dq} = e_q' + j e_d'$ are the stator current, rotor voltage, and transient electromotive force voltage vectors, respectively. $\Delta\omega = \omega - \omega_s$ is the rotor

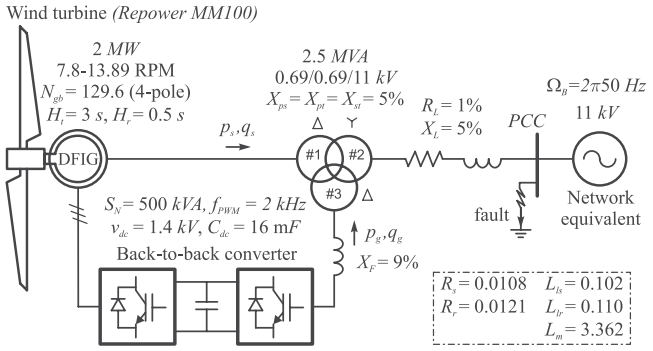

Fig. 1. Schematic representation of a variable-speed WECS based on a DFIG.

slip, R_s, L_s, and L'_s stand for the resistance, self-inductance, and transient inductance of the stator winding, respectively, and τ'_0 is the rotor transient time constant. Expressions (1) and (2) represent the DFIG differential equations (where e'_d and e'_q are dynamic states), whereas the algebraic equations (where i_d and i_q are algebraic states) are

$$0 = -R_s i_d - L'_s i_q + e'_d - v_d \tag{3}$$

$$0 = -R_s i_q + L'_s i_d + e'_q - v_q \tag{4}$$

and $\mathbf{v}_{dq} = v_q + jv_d$ is the stator voltage. Finally, the DFIG stator powers are related to the stator currents by

$$p_s = v_d i_d + v_q i_q \tag{5}$$

$$q_s = v_d i_q - v_q i_d. \tag{6}$$

IV. Straight-Line Control of DFIG Stator Powers

Feedback linearization is a powerful tool to control coupled nonlinear systems. This technique achieves high performance tracking by choosing auxiliary control inputs in a particular way to accomplish an exact linearization in the whole operating range, so that the original system becomes a linear decoupled one. A guideline of the control law derivation is introduced in this section, and further details of the feedback linearization control theory can be consulted in [32]. Equations (5) and (6) show that, by managing the stator currents i_d and i_q, we can directly control the DFIG active and reactive powers. The control outputs i_d and i_q are obtained from the algebraic equations (3) and (4) as

$$i_d = \frac{R_s\left(e'_d - v_d\right) - L'_s\left(e'_q - v_q\right)}{R_s^2 + L_s'^2} \tag{7}$$

$$i_q = \frac{R_s\left(e'_q - v_q\right) + L'_s\left(e'_d - v_d\right)}{R_s^2 + L_s'^2}. \tag{8}$$

First, the DFIG second-order electrical model, given by (1) and (2), along with the control outputs (7) and (8) is written in a matrix form as

$$\dot{\mathbf{x}} = \mathbf{f}(\mathbf{x}) + \mathbf{G}(\mathbf{x})\,\mathbf{u} \tag{9}$$

$$\mathbf{y} = \mathbf{h}(\mathbf{x}) \tag{10}$$

with

$$\mathbf{x} \triangleq [\,e'_q \quad e'_d\,]^T,\ \mathbf{u} \triangleq [\,e_{rd} \quad e_{rq}\,]^T,\ \mathbf{y} \triangleq [\,i_d \quad i_q\,]^T$$

$$\mathbf{f}(\mathbf{x}) \triangleq \begin{bmatrix} \dfrac{-e'_q + (L_s - L'_s)\,i_d}{\tau'_0} - e'_d\Omega_B\Delta\omega \\ \dfrac{-e'_d - (L_s - L'_s)\,i_q}{\tau'_0} + e'_q\Omega_B\Delta\omega \end{bmatrix}$$

$$\mathbf{G}(\mathbf{x}) \triangleq [\,\mathbf{g}_1 \quad \mathbf{g}_2\,] = \frac{1}{\tau'_0}\begin{bmatrix} -1 & 0 \\ 0 & 1 \end{bmatrix}$$

$$\mathbf{h}(\mathbf{x}) \triangleq \begin{bmatrix} h_1 \\ h_2 \end{bmatrix} = \frac{1}{R_s^2 + L_s'^2}\begin{bmatrix} R_s\left(e'_d - v_d\right) - L'_s\left(e'_q - v_q\right) \\ R_s\left(e'_q - v_q\right) + L'_s\left(e'_d - v_d\right) \end{bmatrix}$$

where $\mathbf{x}$, $\mathbf{y}$, and $\mathbf{u}$ are the state, output, and input vectors, respectively. Next, the control law linearizing the system (9), (10) results (see (6.96) in [32] for further details)

$$[\,e_{rd} \quad e_{rq}\,]^T = \mathbf{E}^{-1}(\mathbf{x})\left([\,u_d \quad u_q\,]^T - \mathbf{a}(\mathbf{x})\right) \tag{11}$$

where

$$\mathbf{E}(\mathbf{x}) \triangleq \begin{bmatrix} L_{\mathbf{g}_1}h_1 & L_{\mathbf{g}_2}h_1 \\ L_{\mathbf{g}_1}h_2 & L_{\mathbf{g}_2}h_2 \end{bmatrix}, \quad \mathbf{a}(\mathbf{x}) \triangleq \begin{bmatrix} L_{\mathbf{f}}h_1 \\ L_{\mathbf{f}}h_2 \end{bmatrix}. \tag{12}$$

A simplified notation within Lie derivatives is used, where $L_{\mathbf{f}}h_i = \frac{\partial h_i(\mathbf{x})}{\partial \mathbf{x}}\mathbf{f}$ denotes the Lie derivative of h_i with respect to $\mathbf{f}$ [32]. Then, by considering the DFIG system the matrices of (12) yield

$$\mathbf{E}^{-1} = \tau'_0\begin{bmatrix} L'_s & -R_s \\ R_s & L'_s \end{bmatrix}$$

$$\mathbf{E}^{-1}\mathbf{a} = \begin{bmatrix} \tau'_0\left(R_s i_d + L'_s i_q + v_d\right)\Omega_B\Delta\omega + R_s i_q - L_s i_d + v_q \\ \tau'_0\left(R_s i_q - L'_s i_d + v_q\right)\Omega_B\Delta\omega - R_s i_d - L_s i_q - v_d \end{bmatrix}.$$

Therefore, from (11) the rotor voltages result

$$\begin{aligned} e_{rd} = {} & L_s i_d - R_s i_q - v_q + \tau'_0\left(L'_s u_d - R_s u_q\right) \\ & - \tau'_0\left(R_s i_d + L'_s i_q + v_d\right)\Omega_B\Delta\omega \end{aligned} \tag{13}$$

$$\begin{aligned} e_{rq} = {} & L_s i_q + R_s i_d + v_d + \tau'_0\left(L'_s u_q + R_s u_d\right) \\ & - \tau'_0\left(R_s i_q - L'_s i_d + v_q\right)\Omega_B\Delta\omega. \end{aligned} \tag{14}$$

Finally, by differentiating with respect to time the control outputs i_d and i_q, from (7) and (8), and using the control law (13) and (14), the following two decoupled first-order linear systems are obtained:

$$\dot{i}_d = u_d \tag{15}$$

$$\dot{i}_q = u_q. \tag{16}$$

This makes it easier to design the auxiliary control signals u_d and u_q, as it will be developed in the next section.

At this point, it is worthy to deal with an eigenvalue analysis which exposes the marginal stability issue. The eigenvalue movement of the closed-loop system when increasing the control gain is presented in Fig. 2. An approach controlling the DFIG stator currents using the fourth-order electric model is represented with square marks. The proposed approach using the simplified second-order electric model is shown with solid

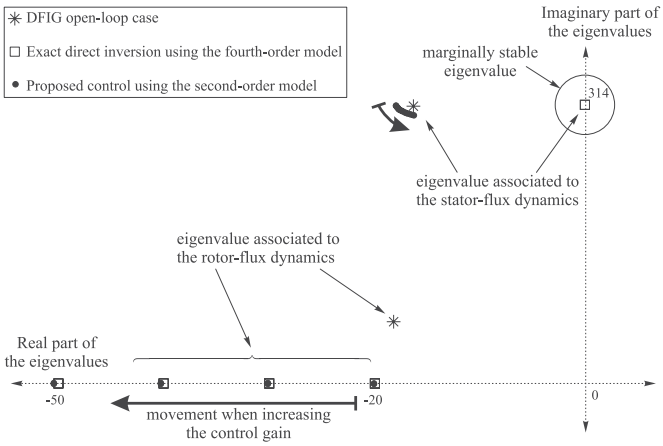

Fig. 2. Small signal analysis: eigenvalue movement for two control approaches when their control gain is increased.

circle marks, and the eigenvalues of the open-loop case are shown with asterisk marks. When increasing the control gain, for both control approaches, the eigenvalue associated with the rotor-flux dynamics can be damped and placed in a desired location. However, the first scheme makes the eigenvalue associated with the stator-flux dynamics to have a real part equal to zero (marginal stability) for all control gains. On the other hand, the proposed approach allows us to impose a desired rotor-flux dynamics, and almost does not affect the stator-flux dynamics. This results in a stable DFIG operation and a high-performance and implementable controller, as will be shown in Section VII.

V. Control Design to Ride-Through Distorted and Unbalanced Conditions

A. Dynamic Extension of the System

After the input transformations (13) and (14), the DFIG electric model was simplified to a pair of decoupled first-order linear systems (15) and (16). Note that these systems have a structure of the general form $\dot{x} = u$, or in the Laplace domain $G(s) = \frac{X(s)}{U(s)} = \frac{1}{s}$, which can be digitized by using the zero-order hold (ZOH) discretization as follows [33]:

$$\frac{X(z)}{U(z)} = \left(1 - z^{-1}\right) \mathcal{Z}\left\{\frac{1}{s} G(s)\right\} = \frac{T_s}{z-1} \tag{17}$$

where $\mathcal{Z}$ stands for the z-transform and T_s is the control sampling time. The discrete system transfer function (17) can be written in a state-space representation as

$$x_{k+1} = x_k + T_s u_k. \tag{18}$$

In order to build the control signal u_k, the following must be taken into account. In general, the grid voltage can be considered as a sum of several frequencies. For instance, the main components are $+\omega$ (fundamental), $-\omega$ (imbalance), -5ω, $+7\omega$, -11ω, $+13\omega$, ... (harmonics). In a reference frame rotating to the synchronous speed, the aforementioned frequency components are shifted to 0ω (dc component), 2ω, $\pm 6\omega$, $\pm 12\omega$, ..., etc. A PI controller could be implemented to track dc components; however, to guarantee a null steady-state error for 2ω components and a rejection of harmonic components in the PCC voltage, resonant filters (high gain paths) should be added to the controller, with resonant frequencies at 2ω (imbalances), $\pm 6\omega$ (harmonics -5ω and $+7\omega$), $\pm 12\omega$ (harmonics -11ω and $+13\omega$), etc. In the continuous time domain, a resonant filter with resonant frequency ω_r is given by

$$G_r(s) = \frac{s}{s^2 + \omega_r^2}. \tag{19}$$

A discrete state-space representation of the continuous transfer function (19) can be obtained either by using a discretization via the ZOH method (further details of the ZOH discretization can be consulted in [33]) or by using the "c2d" command of MATLAB. Then, it results

$$\mathbf{h}_{k+1}^{\omega_r} = \mathbf{A}^{\omega_r} \mathbf{h}_k^{\omega_r} + \mathbf{B}^{\omega_r} s_k \tag{20}$$

where

$$\mathbf{h}_k^{\omega_r} \triangleq \begin{bmatrix} x_{1k} & x_{2k} \end{bmatrix}^T \tag{21}$$

$$\mathbf{A}^{\omega_r} \triangleq \begin{bmatrix} 0 & -1 \\ 1 & 2\cos(\omega_r T_s) \end{bmatrix} \tag{22}$$

$$\mathbf{B}^{\omega_r} \triangleq \frac{\sin(\omega_r T_s)}{\omega_r} \begin{bmatrix} -1 \\ 1 \end{bmatrix}. \tag{23}$$

The current tracking error is denoted as $s_k = x_k - x_k^\star$, where $x_k^\star$ indicates the reference current value. By combining the system model (18), the PI regulator, and the resonant filters at frequencies 2ω, 6ω, and 12ω [using the resonant model (20)], we can obtain an extended system model as follows:

$$\mathbf{w}_{k+1} = \mathbf{A}\mathbf{w}_k + \mathbf{B}u_k - \mathbf{B}_r x_k^\star \tag{24}$$

where the following vectors and matrices are defined:

$$\mathbf{w}_k \triangleq \begin{bmatrix} x_k & \eta_k & \mathbf{h}_k^{\omega_2} & \mathbf{h}_k^{\omega_6} & \mathbf{h}_k^{\omega_{12}} \end{bmatrix}^T \tag{25}$$

$$\mathbf{A} \triangleq \begin{bmatrix} 1 & 0 & \mathbf{0} & \mathbf{0} & \mathbf{0} \\ T_s & 1 & \mathbf{0} & \mathbf{0} & \mathbf{0} \\ \mathbf{B}^{\omega_2} & \mathbf{0} & \mathbf{A}^{\omega_2} & \mathbf{0} & \mathbf{0} \\ \mathbf{B}^{\omega_6} & \mathbf{0} & \mathbf{0} & \mathbf{A}^{\omega_6} & \mathbf{0} \\ \mathbf{B}^{\omega_{12}} & \mathbf{0} & \mathbf{0} & \mathbf{0} & \mathbf{A}^{\omega_{12}} \end{bmatrix} \tag{26}$$

$$\mathbf{B} \triangleq \begin{bmatrix} T_s & 0 & \mathbf{0} & \mathbf{0} & \mathbf{0} \end{bmatrix}^T \tag{27}$$

$$\mathbf{B}_r \triangleq \begin{bmatrix} 0 & T_s & \mathbf{B}^{\omega_2} & \mathbf{B}^{\omega_6} & \mathbf{B}^{\omega_{12}} \end{bmatrix}^T. \tag{28}$$

The new extended state vector $\mathbf{w}_k$ is built with the system state x_k (stator current i_d or i_q), the integrator state of the PI η_k, and the internal states $\mathbf{h}_k^{\omega_2}$, $\mathbf{h}_k^{\omega_6}$, and $\mathbf{h}_k^{\omega_{12}}$ of the resonant filters 2ω, 6ω, and 12ω, respectively. If it would be necessary to consider more harmonics for a particular application, they could be simply added in the diagonal of the matrix $\mathbf{A}$, in (26). This extended system allows us to calculate the control input u_k using a state-space design method. Therefore, the control input u_k is obtained feeding back all the extended states

$$u_k = -\mathbf{K}\mathbf{w}_k + K_r x_k^\star \tag{29}$$

where $\mathbf{K}$ is the control gain matrix and $K_r = \mathbf{K}(1)$. Then, by replacing the control law (29) in the extended system (24), the

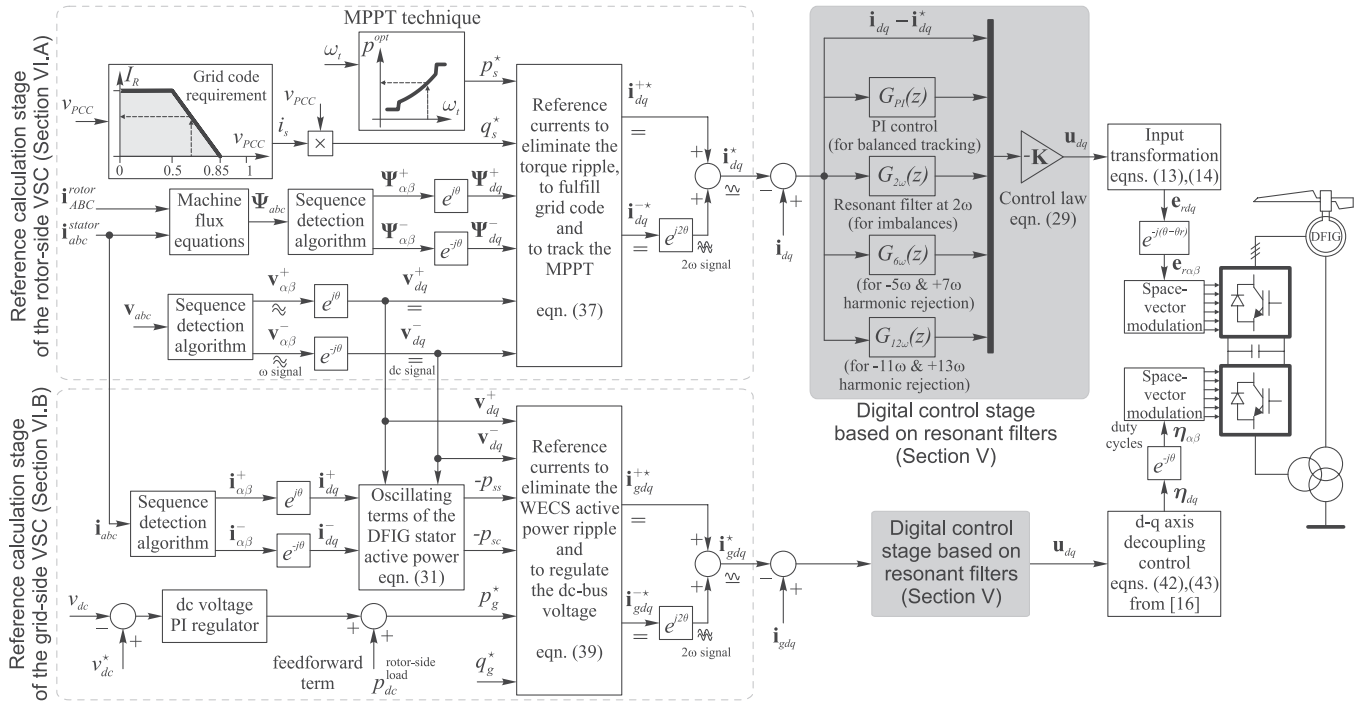

Fig. 3. Block diagram showing the implementation of the proposed strategy as well as the different stages of both rotor- and grid-side converter controls.

closed-loop system is obtained as

$$\mathbf{w}_{k+1} = (\mathbf{A} - \mathbf{BK})\,\mathbf{w}_k + (\mathbf{B}K_r - \mathbf{B}_r)\,x_k^\star. \tag{30}$$

B. Control Gain Synthesis

The feedback gain matrix $\mathbf{K}$ is chosen so that the matrix $(\mathbf{A} - \mathbf{BK})$ is stable and gives a desired closed-loop system response. This can be made by using linear techniques such as the optimal quadratic regulation [33]. The optimal control gain is obtained by minimizing the cost function $J = \sum_{k=1}^{\infty} \left(\mathbf{w}_k^T \mathbf{Q} \mathbf{w}_k + u_k^T R u_k\right)$. This index J could be easily minimized by using the "dlqr" command of MATLAB.

A block diagram of the whole control scheme is presented in Fig. 3, where the different stages of the strategy are shown.

VI. Reference Current Calculation

A. Reference Currents of the Rotor-Side Converter

Under unbalanced conditions, the DFIG stator apparent power can be partitioned as follows [13], [26], [34]:

$$\begin{aligned}\mathbf{s}_s &= \frac{2}{3}\mathbf{v}_{abc}\mathbf{i}_{abc}^* \\ &= \left(\mathbf{v}_{dq}^+ e^{j\omega_s t} + \mathbf{v}_{dq}^- e^{-j\omega_s t}\right)\left(\mathbf{i}_{dq}^+ e^{j\omega_s t} + \mathbf{i}_{dq}^- e^{-j\omega_s t}\right)^* \\ &= (p_s + p_{ss}\sin 2\omega_s t + p_{sc}\cos 2\omega_s t) + \\ &\quad + j\,(q_s + q_{ss}\sin 2\omega_s t + q_{sc}\cos 2\omega_s t)\end{aligned} \tag{31}$$

where p_s and q_s are the constant (dc) components of the stator active and reactive powers, whereas p_{ss}, p_{sc}, q_{ss}, and q_{sc} are the amplitude of the sine and cosine 2ω oscillation terms of active and reactive powers, respectively. Symbols $(+)$, $(-)$, and $(*)$ are used to indicate a positive sequence, negative sequence, and conjugated value, respectively.

Likewise, the electromagnetic torque of the machine can be written as (see [13] and [35])

$$\begin{aligned}\tau_e &= -\frac{2}{3}\mathrm{Im}\left\{\psi_{abc}\mathbf{i}_{abc}^*\right\} \\ &= \tau_{e0} + \tau_{es}\sin 2\omega_s t + \tau_{ec}\cos 2\omega_s t.\end{aligned} \tag{32}$$

Expanding the current and voltage vectors in (31) and (32), the following relations are obtained:

$$p_s = i_d^- v_d^- + i_d^+ v_d^+ + i_q^- v_q^- + i_q^+ v_q^+ \tag{33}$$

$$q_s = i_q^- v_d^- + i_q^+ v_d^+ - i_d^- v_q^- - i_d^+ v_q^+ \tag{34}$$

$$\tau_{es} = i_d^- \psi_d^+ - i_d^+ \psi_d^- - i_q^+ \psi_q^- + i_q^- \psi_q^+ \tag{35}$$

$$\tau_{ec} = i_q^- \psi_d^+ + i_q^+ \psi_d^- - i_d^+ \psi_q^- - i_d^- \psi_q^+. \tag{36}$$

In order to eliminate the 2ω ripple in the electromagnetic torque, its oscillating terms in (32) must be nullified ($\tau_{es} = \tau_{ec} = 0$). On the other hand, the reference of the DFIG active power $p_s^\star$ is obtained from a maximum power point tracking (MPPT) algorithm which, by using a lookup table of the turbine maximum power curve and measuring the rotor speed, gets the optimal active power [21]. The reference of the reactive power $q_s^\star$ injected by the DFIG is calculated from a typical grid code curve (see the right-side plot in Fig. 5) which relates the injection of reactive current with the voltage amplitude at the PCC [4], [36]. Taking into account these considerations, from the equation system (33)–(36), the reference currents of the rotor-side converter are

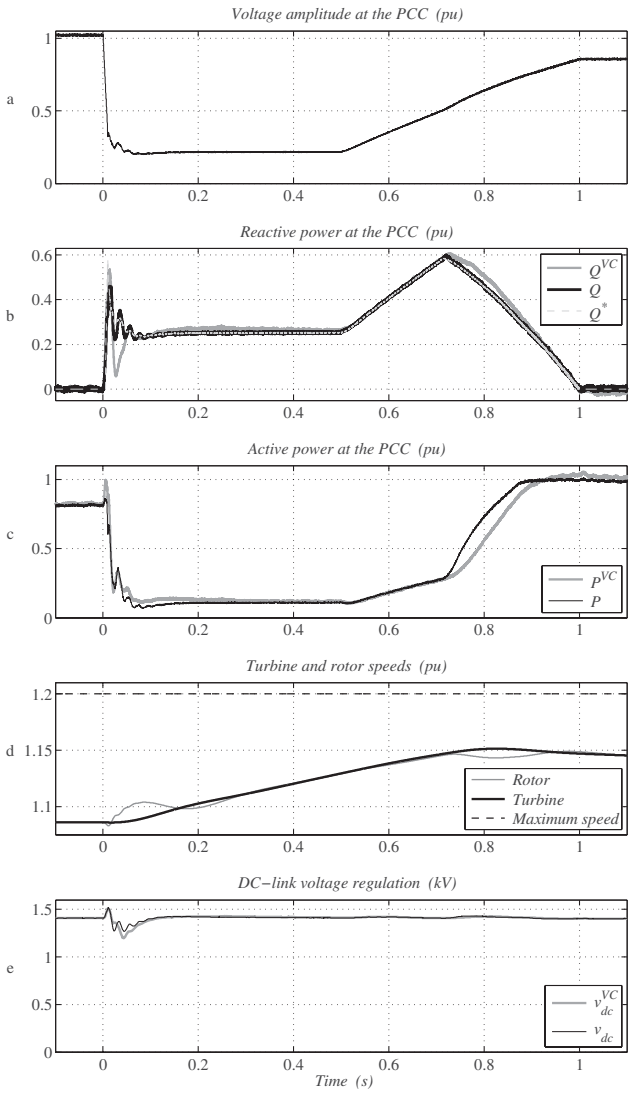

Fig. 4. Three-phase fault test with standard voltage sag (from the Spanish grid code [36]), and the behavior of the main WECS variables.

obtained as

$$\begin{bmatrix} i_d^{+\star} \\ i_q^{+\star} \\ i_d^{-\star} \\ i_q^{-\star} \end{bmatrix} = \begin{bmatrix} v_d^+ & v_q^+ & v_d^- & v_q^- \\ -v_q^+ & v_d^+ & -v_q^- & v_d^- \\ -\psi_d^- & -\psi_q^- & \psi_d^+ & \psi_q^+ \\ -\psi_q^- & \psi_d^- & -\psi_q^+ & \psi_d^+ \end{bmatrix}^{-1} \begin{bmatrix} p_s^\star \\ q_s^\star \\ 0 \\ 0 \end{bmatrix}. \quad (37)$$

If the stator currents follow the aforementioned references, the active and reactive powers injected by the DFIG will be $p_s^\star$ and $q_s^\star$, whereas the 2ω pulsations in the electromagnetic torque will be eliminated. To accomplish these objectives, we use all the control freedom degrees of the rotor-side converter; in the next subsection, we will coordinate the rotor-side and grid-side converters to nullify the 2ω pulsations in the total active power injected by the WECS under unbalanced conditions.

B. Reference Currents of the Grid-Side Converter

The apparent power injected by the grid-side converter to the grid can be partitioned as follows [37]:

$$\begin{aligned} \mathbf{s}_g &= \frac{2}{3}\mathbf{v}_{abc}\mathbf{i}_{gabc}^* \\ &= (p_g + p_{gs}\sin 2\omega_s t + p_{gc}\cos 2\omega_s t) \\ &\quad + j\,(q_g + q_{gs}\sin 2\omega_s t + q_{gc}\cos 2\omega_s t)\,. \end{aligned} \quad (38)$$

The total WECS power is the sum of the powers from the grid-side converter and the DFIG stator. Then, to eliminate the 2ω pulsations in the total WECS active power, we need to inject with the grid-side converter the opposite 2ω oscillating active power which delivers the DFIG stator ($p_{gs} = -p_{ss}$ and $p_{gc} = -p_{sc}$). Consequently, by proceeding as in the above subsection, the reference currents of the grid-side converter can be obtained as follows:

$$\begin{bmatrix} i_{gd}^{+\star} \\ i_{gq}^{+\star} \\ i_{gd}^{-\star} \\ i_{gq}^{-\star} \end{bmatrix} = \begin{bmatrix} v_d^+ & v_q^+ & v_d^- & v_q^- \\ -v_q^+ & v_d^+ & -v_q^- & v_d^- \\ -v_q^- & v_d^- & v_q^+ & -v_d^+ \\ v_d^- & v_q^- & v_d^+ & v_q^+ \end{bmatrix}^{-1} \begin{bmatrix} p_g^\star \\ q_g^\star \\ -p_{ss} \\ -p_{sc} \end{bmatrix}. \quad (39)$$

The reference of the active power $p_g^\star$ is obtained from a PI regulator which controls the dc-link voltage, whereas the reactive power $q_g^\star$ contributes to compensate the reactive consumption of the step-up transformer, lines, and cables which connect the windmill to the PCC.

Matrices in (37) and (39) are singular when the squared magnitude of the negative-sequence voltage equals the positive-sequence voltage, i.e., $(v_d^{+\,2} + v_q^{+\,2}) - (v_d^{-\,2} + v_q^{-\,2}) = 0$ (see [13], [38], [39] where similar equations were used). However, this is a quite extreme case of unbalanced voltage, and, in such cases, a limited action of the ripple elimination should be performed not to exceed transient or normal operating ranges of the machine and converters [35].

Unlike the controller stage designed in Section V where, by using resonant filters, we allowed to track 2ω-signal references and to reject grid harmonics, at this reference calculation stage, a sequence detection algorithm is required to obtain the positive- and negative-sequence voltages needed to compute (37) and (39). Fig. 3 shows where the resonant filters and the sequence detention algorithm are used. The required extraction of the positive- and negative-sequence components is accomplished by using the technique described in [40].

VII. Performance Testing

This section presents the most relevant results regarding the assessment of the proposed strategy. The system and controller are implemented in the SimPowerSystems blockset of SIMULINK/MATLAB. The power system configuration and data used in tests are shown in Fig. 1. The control parameters are $\mathbf{K} = [\ 984\ 108\ 541\ -548\ 725\ -793\ ]$, $K_r = 984$, and gains of the dc voltage PI regulator $K_p = 0.35$ and $K_i = 1.75$. Outer-loop PI control was synthesized according to the guidelines presented in [21] and [41] using MATLAB SISO tools. The

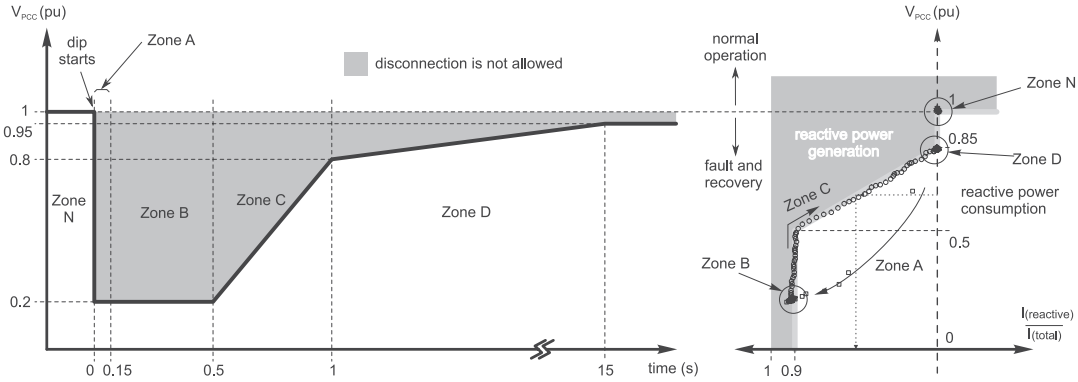

Fig. 5. Standard voltage sag waveform (left-side plot) and the grid code curve which gives the reactive current injection as a function of the PCC voltage (right-side plot), both from the Spanish grid code [36].

simulation conditions are wind speed $v_w = 10$ m/s, mechanical torque $T_m = 0.8$ pu, and turbine speed $\omega_t = 12.57$ RPM.

To analyze the controller robustness, it is assumed that its machine parameters are different from the actual plant parameters. A 20% error is considered for the mutual inductance, L_m (similar results are obtained for an error of -20%). Analyzing this error is relevant because several DFIG parameters such as L_s=L_m+L_{ls}, L_r=L_m+L_{lr}, L'_s=$L_s - \frac{L_m^2}{L_r}$ and $\tau'_0 = \frac{L_r}{\Omega_B R_r}$ depend on this parameter. A 30% error in the stator resistance is also considered.

A. FRT and Grid Code Compliance

A three-phase fault test with standard voltage sag, from the Spanish grid code [36], is performed to evaluate the FRT capability and the grid code fulfillment. Fig. 4(a) shows the voltage amplitude at the PCC bus. This is a hard requirement, as the low-voltage condition puts the system at an operating state which is far from the normal one. Moreover, the grid code demands the WECS not only to remain connected but also to deliver reactive power to the grid in order to support the voltage recovery [see the dashed line Q^* in Fig. 4(b)]. For comparison purposes, in Fig. 4(b) the injected reactive power using the proposed scheme (dark line Q) and a conventional VC (light line Q^{VC}) is plotted. The proposed scheme follows the reference power more accurately than the VC, especially at the beginning of the fault where synchronization with the stator flux and PI tuning of the VC lose some performance. The active power injected by the WECS during the fault is given in Fig. 4(c). In Fig. 4(d) an increase in the turbine and rotor speeds can be observed, since the low-voltage condition does not allow exporting all the wind mechanical power. However, it only arises to $+15\%$, where a DFIG-based WECS can normally reach up to $\pm 20\%$ of the synchronous speed. Finally, Fig. 4(e) presents the dc-link voltage control during the fault period. A good dc voltage regulation is performed by both schemes, although some little more overshoot at the beginning of the fault is seen in the VC.

Fig. 5 shows the profile of the PCC voltage amplitude (left-side plot) and the grid code curve which gives the reactive current injection as a function of the PCC voltage (right-side plot). In the latter plot, the WECS operating points throughout the period of interest are included with markers. It is seen there that the system fulfills the grid code requirements when the proposed strategy is adopted. We defined five zones named N, A, B, C, and D to easily connect both right- and left-side plots.

B. Unbalanced Test and Elimination of 2ω Pulsations

A test involving an unbalanced grid voltage [see Fig. 6(a)], produced by a near asymmetrical load or fault, is accomplished to highlight the controller features of eliminating 2ω pulsations. At the test beginning, the DFIG control does not have any ripple elimination characteristics activated (as in a conventional strategy); at t=0.15 s the feature to eliminate the electromagnetic torque ripple is included, and then, at t=0.30 s, the elimination feature of the active power ripple is also connected. It is shown in Fig. 6(b) that, before t=0.15 s, the DFIG electromagnetic torque has a 20% peak-to-peak ripple due to the unbalanced condition but, after the activation of the elimination feature, the electromagnetic torque ripple is completely nullified. Fig. 6(c) shows the total WECS active power injected to the grid. There, we also observe that large 2ω pulsations are present in the active power but, after the compensation feature is activated at t=0.30 s, these pulsations are removed. An additional advantage when ripple elimination of the torque and power is simultaneously achieved at t=0.30 s is that the 2ω-ripple of the dc-link voltage is highly reduced as well (see Fig. 6(d) after t=0.30 s). The rotor, stator, and grid-side current waveforms needed to attain the aforementioned elimination objectives are plotted in Fig. 6(e)–(g), respectively.

C. Harmonic Rejection Capability

This last test is introduced to analyze the controller performance when harmonics are present in the grid voltage. At the test beginning, neither harmonics in the grid voltage nor the harmonic rejection capability is included. At t=0.02 s, 12% of fifth and 7% of seventh harmonics are added to the grid voltage [as shown in Fig. 7(a)], and then, at t=0.07s, the harmonic rejection capability is connected. This test evaluates the DFIG behavior with and without the proposed scheme. Fig. 7(b) shows the high distortion in the DFIG stator currents before t=0.07 s, when the controller with harmonic rejection capability is not implemented (as in a conventional strategy). On the

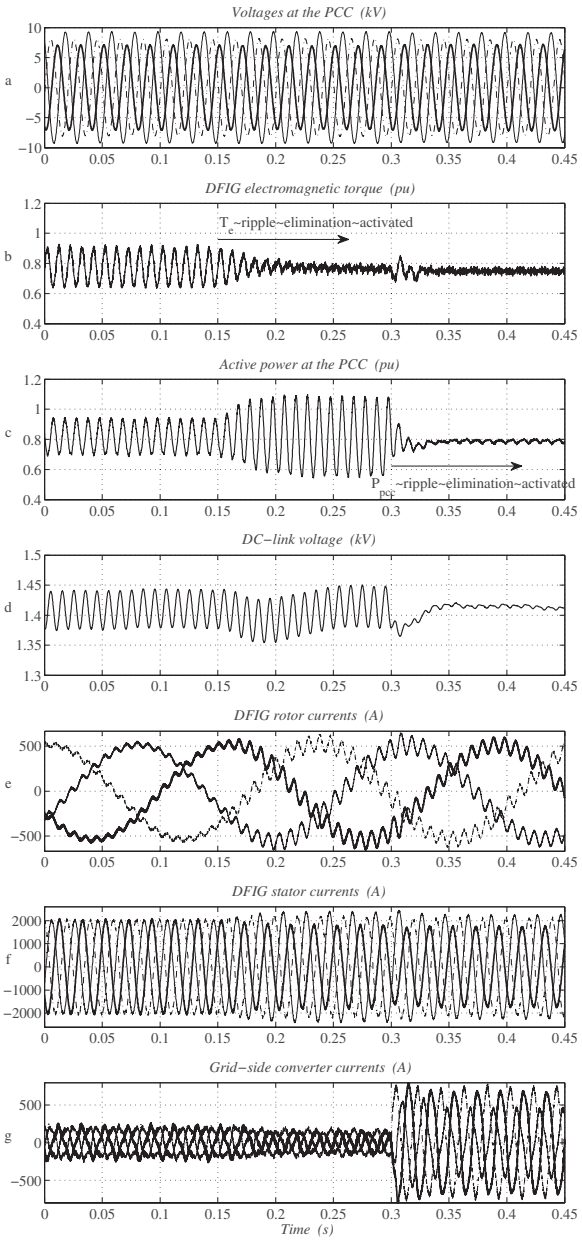

Fig. 6. Test with an unbalanced grid voltage and 2ω-ripple elimination.

other hand, in Fig. 7(b), after the harmonic rejection capability is activated at t=0.07 s, the DFIG currents become perfectly sinusoidal and harmonic-free. The rotor voltages and currents needed to attain the aforementioned harmonic rejection are plotted in Fig. 7(c) and (d), respectively.

VIII. Conclusion

A DFIG control strategy able to precisely control the active and reactive powers delivered by WECSs was proposed in this study. This strategy fulfills severe FRT conditions and grid code requirements, and overcomes various network disturbances. The DFIG stator powers were directly controlled using a feedback linerization plus resonant control to ride-through unbalanced and harmonic distortions at the PCC. Double-frequency pulsations in the total WECS active power, electromagnetic torque,

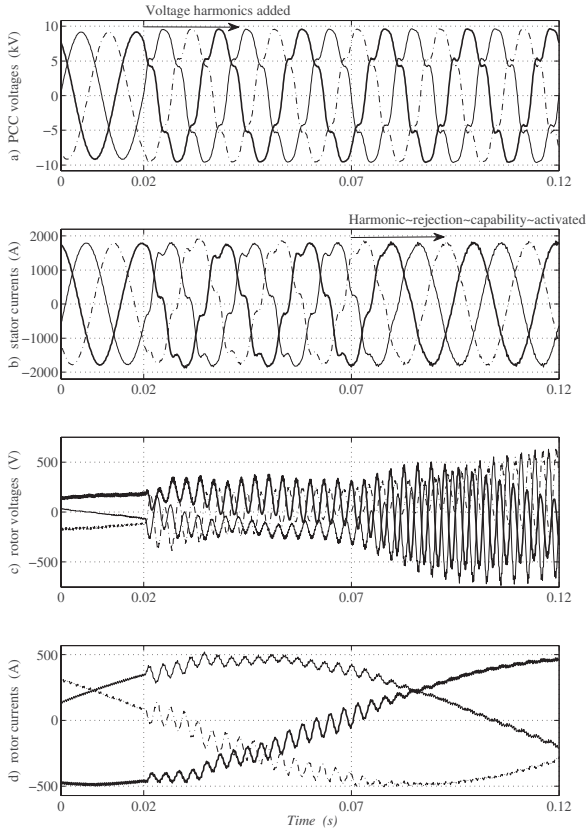

Fig. 7. Harmonic rejection capability under a distorted grid voltage.

and dc-link voltage were simultaneously reduced by coordinating the grid- and rotor-side converter controls. Several tests, disturbances, and comparisons with conventional strategies were performed to illustrate the adequacy and advantages of the presented strategy.

References

[1] M. Liserre, R. Cardenas, M. Molinas, and J. Rodriguez, "Overview of multi-MW wind turbines and wind parks," *IEEE Trans. Ind. Electron.*, vol. 58, no. 4, pp. 1081–1095, Apr. 2011.

[2] F. M. Hughes, O. Anaya-Lara, N. Jenkins, and G. Strbac, "Control of DFIG-based wind generation for power network support," *IEEE Trans. Power Syst.*, vol. 20, no. 4, pp. 1958–1966, Nov. 2005.

[3] A. Ibrahim, T. H. Nguyen, D.-C. Lee, and S.-C. Kim, "A fault ride-through technique of DFIG wind turbine systems using dynamic voltage restorers," *IEEE Trans. Energy Convers.*, vol. 26, no. 3, pp. 871–882, Sep. 2011.

[4] A. E. Leon, J. M. Mauricio, A. Gomez-Exposito, and J. A. Solsona, "An improved control strategy for hybrid wind farms," *IEEE Trans. Sustainable Energy*, vol. 1, no. 3, pp. 131–141, Oct. 2010.

[5] O. Anaya-Lara, F. Hughes, N. Jenkins, and G. Strbac, "Contribution of DFIG-based wind farms to power system short-term frequency regulation," *Proc. Inst. Elect. Eng., Gener., Transm. Distrib*, vol. 153, no. 2, pp. 164–170, Mar. 2006.

[6] J. Mauricio, A. Marano, A. Gomez-Exposito, and J. Martinez Ramos, "Frequency regulation contribution through variable-speed wind energy conversion systems," *IEEE Trans. Power Syst.*, vol. 24, no. 1, pp. 173–180, Feb. 2009.

[7] N. R. Ullah and T. Thiringer, "Variable speed wind turbines for power system stability enhancement," *IEEE Trans. Energy Convers.*, vol. 22, no. 1, pp. 52–60, Mar. 2007.

[8] G. Tsourakis, B. M. Nomikos, and C. D. Vournas, "Contribution of doubly fed wind generators to oscillation damping," *IEEE Trans. Energy Convers.*, vol. 24, no. 3, pp. 783–791, Sep. 2009.

[9] S. Z. Chen, N. Cheung, Y. Zhang, M. Zhang, and X. M. Tang, "Improved

grid synchronization control of doubly fed induction generator under unbalanced grid voltage," *IEEE Trans. Energy Convers.*, vol. 26, no. 3, pp. 799–810, Sep. 2011.
[10] L. Xu and Y. Wang, "Dynamic modeling and control of DFIG-based wind turbines under unbalanced network conditions," *IEEE Trans. Power Syst.*, vol. 22, no. 1, pp. 314–323, Feb. 2007.
[11] T. K. A. Brekken and N. Mohan, "Control of a doubly fed induction wind generator under unbalanced grid voltage conditions," *IEEE Trans. Energy Convers.*, vol. 22, no. 1, pp. 129–135, Mar. 2007.
[12] N. Joshi and N. Mohan, "A novel scheme to connect wind turbines to the power grid," *IEEE Trans. Energy Convers.*, vol. 24, no. 2, pp. 504–510, Jun. 2009.
[13] A. G. Abo-Khalil, D.-C. Lee, and J.-I. Jang, "Control of back-to-back PWM converters for DFIG wind turbine systems under unbalanced grid voltage," *Proc. IEEE Int. Symp. Ind. Elect.*, pp. 2637–2642, Jun. 2007.
[14] E. Tremblay, S. Atayde, and A. Chandra, "Comparative study of control strategies for the doubly fed induction generator in wind energy conversion systems: A DSP-based implementation approach," *IEEE Trans. Sustainable Energy*, vol. 2, no. 3, pp. 288–299, Jul. 2011.
[15] L. Yang, Z. Xu, J. Ostergaard, Z. Y. Dong, K. P. Wong, and X. Ma, "Oscillatory stability and eigenvalue sensitivity analysis of a DFIG wind turbine system," *IEEE Trans. Energy Convers.*, vol. 26, no. 1, pp. 328–339, Mar. 2011.
[16] J. M. Mauricio, A. E. Leon, A. Gomez-Exposito, and J. A. Solsona, "An adaptive nonlinear controller for DFIM-based wind energy conversion systems," *IEEE Trans. Energy Convers.*, vol. 23, no. 4, pp. 1025–1035, Dec. 2008.
[17] R. Cardenas, R. Pena, J. Proboste, G. Asher, and J. Clare, "MRAS observer for sensorless control of standalone doubly fed induction generators," *IEEE Trans. Energy Convers.*, vol. 20, no. 4, pp. 710–718, Dec. 2005.
[18] L. Xu, "Coordinated control of DFIG's rotor and grid side converters during network unbalance," *IEEE Trans. Power Electron.*, vol. 23, no. 3, pp. 1041–1049, May 2008.
[19] A. Luna, K. Lima, F. Corcoles, E. Watanabe, P. Rodriguez, and R. Teodorescu, "Control of DFIG-WT under unbalanced grid voltage conditions," in *Proc. IEEE Energy Convers. Congr. Expo.*, Sep. 2009, pp. 370–377.
[20] A. Tapia, G. Tapia, J. X. Ostolaza, and J. R. Sáenz, "Modeling and control of a wind turbine driven doubly fed induction generator," *IEEE Trans. Energy Convers.*, vol. 18, no. 2, pp. 194–204, Jun. 2003.
[21] R. Pena, J. Clare, and G. Asher, "Doubly fed induction generator using back-to-back PWM converters and its application to variable-speed wind-energy generation," *Proc. Inst. Elect. Eng., Elect. Power Appl.*, vol. 143, no. 3, pp. 231–241, May 1996.
[22] B. Hopfensperger, D. Atkinson, and R. Lakin, "Stator-flux-oriented control of a doubly-fed induction machine with and without position encoder," *Proc. Inst. Elect. Eng., Elect. Power Appl.*, vol. 147, no. 4, pp. 241–250, Jul. 2000.
[23] S. Peresada, A. Tilli, and A. Tonielli, "Power control of a doubly fed induction machine via output feedback," *Control Eng. Practice*, vol. 12, no. 1, pp. 41–57, 2004.
[24] C. Batlle, A. Doria-Cerezo, and R. Ortega, "Power flow control of a doubly-fed induction machine coupled to a flywheel," in *Proc. IEEE Inter. Conf. Control Appl.*, Sep. 2004, vol. 2, pp. 1645–1650.
[25] F. Wu, X.-P. Zhang, P. Ju, and M. Sterling, "Decentralized nonlinear control of wind turbine with doubly fed induction generator," *IEEE Trans. Power Syst.*, vol. 23, no. 2, pp. 613–621, May 2008.
[26] J. Hu, Y. He, L. Xu, and B. W. Williams, "Improved control of DFIG systems during network unbalance using PI-R current regulators," *IEEE Trans. Ind. Electron.*, vol. 56, no. 2, pp. 439–451, Feb. 2009.
[27] D. Xiang, L. Ran, P. Tavner, and S. Yang, "Control of a doubly fed induction generator in a wind turbine during grid fault ride-through," *IEEE Trans. Energy Convers.*, vol. 21, no. 3, pp. 652–662, Sep. 2006.
[28] J. Hu, H. Nian, H. Xu, and Y. He, "Dynamic modeling and improved control of DFIG under distorted grid voltage conditions," *IEEE Trans. Energy Convers.*, vol. 26, no. 1, pp. 163–175, Mar. 2011.
[29] A. Feijoo, J. Cidras, and C. Carrillo, "A third order model for the doubly-fed induction machine," *Elect. Power Syst. Res.*, vol. 56, no. 2, pp. 121–127, 2000.
[30] J. Ekanayake, L. Holdsworth, and N. Jenkins, "Comparison of 5th order and 3rd order machine models for doubly fed induction generator (DFIG) wind turbines," *Elect. Power Syst. Res.*, vol. 67, no. 3, pp. 207–215, 2003.
[31] Y. Lei, A. Mullane, G. Lightbody, and R. Yacamini, "Modeling of the wind turbine with a doubly fed induction generator for grid integration studies," *IEEE Trans. Energy Convers.*, vol. 21, no. 1, pp. 257–264, Mar. 2006.
[32] J.-J. E. Slotine and W. Li, *Applied Nonlinear Control*. Englewood Cliffs, NJ: Prentice-Hall, 1991.
[33] K. Ogata, *Discrete-Time Control Systems*, 2nd ed. Englewood Cliffs, NJ: Prentice-Hall, 1995.
[34] H. Nian, Y. Song, P. Zhou, and Y. He, "Improved direct power control of a wind turbine driven doubly fed induction generator during transient grid voltage unbalance," *IEEE Trans. Energy Convers.*, vol. 26, no. 3, pp. 976–986, Sep. 2011.
[35] S. Engelhardt, I. Erlich, C. Feltes, J. Kretschmann, and F. Shewarega, "Reactive power capability of wind turbines based on doubly fed induction generators," *IEEE Trans. Energy Convers.*, vol. 26, no. 1, pp. 364–372, Mar. 2011.
[36] Red Eléctrica. P.O. 12.3. (2006, Oct.) "Requirements of the response against voltage sags by special regime generation assets (in spanish)," *Spanish Ministry Ind., Tourism Commerce. BOE Núm. 254.*, pp. 1–7. [online]. Available: http://www.ree.es
[37] A. E. Leon, J. M. Mauricio, J. A. Solsona, and A. Gomez-Exposito, "Adaptive control strategy for VSC-based systems under unbalanced network conditions," *IEEE Trans. Smart Grid*, vol. 1, no. 3, pp. 311–319, Dec. 2010.
[38] H.-S. Song and K. Nam, "Dual current control scheme for PWM converter under unbalanced input voltage conditions," *IEEE Trans. Ind. Electron.*, vol. 46, no. 5, pp. 953–959, Oct. 1999.
[39] I. Etxeberria-Otadui, U. Viscarret, M. Caballero, A. Rufer, and S. Bacha, "New optimized PWM VSC control structures and strategies under unbalanced voltage transients," *IEEE Trans. Ind. Electron.*, vol. 54, no. 5, pp. 2902–2914, Oct. 2007.
[40] K. Selvajyothi and P. A. Janakiraman, "Extraction of harmonics using composite observers," *IEEE Trans. Power Del.*, vol. 23, no. 1, pp. 31–40, Jan. 2008.
[41] H. Nikkhajoei and R. Iravani, "Dynamic model and control of AC/DC/AC voltage-sourced converter system for distributed resources," *IEEE Trans. Power Del.*, vol. 22, no. 2, pp. 1169–1178, Apr. 2007.

Andres E. Leon (GS'05) was born in Argentina in 1979. He received the Electrical Engineering degree from the Universidad Nacional del Comahue, Neuquén, Argentina, and the Ph.D. degree from the Universidad Nacional del Sur, Bahía Blanca, Argentina, in 2005 and 2011, respectively.

He is currently a researcher at the Instituto de Investigaciones en Ingeniería Eléctrica "Alfredo Desages" (IIIE-CONICET), Bahía Blanca. His primary research interests include power system control, custom power systems, and wind energy conversion systems.

Juan Manuel Mauricio (M'07) was born in Argentina in 1977. He received the Electrical Engineering degree from the National University of Comahue, Neuquén, Argentina, in 2003, and the Master and Doctor Engineering degrees from the University of Seville, Seville, Spain, in 2007 and 2009, respectively.

Since 2004 he has been with the Department of Electrical Engineering, University of Seville, where he is currently an Assistant Professor. His primary research interests include power systems and electrical machine control, renewable generation, voltage source converters-based applications, and electrical vehicles.

Jorge A. Solsona (SM'04) received the electronics engineer and Dr. degrees from the Universidad Nacional de La Plata, La Plata, Argentina, in 1986 and 1995, respectively.

He is currently with the Instituto de Investigaciones en Ingeniería Eléctrica Alfredo Desages (IIIE), Departamento de Ingeniería Eléctrica y de Computadoras, Universidad Nacional del Sur, Bahía Blanca, Argentina, and CONICET where he is involved in teaching and research on control theory and its applications to electromechanical systems.